Phonon spectrum and electron-phonon coupling in zigzag graphene nanoribbons

Ting Zhang,[1,2,3,*] Rolf Heid,[2] Klaus-Peter Bohnen,[2] Ping Sheng,[1,3] and C. T. Chan[1,3]

[1]*Department of Physics, Hong Kong University of Science and Technology, Clear Water Bay, Kowloon, Hong Kong, China*

[2]*Institut für Festkörperphysik, Karlsruher Institut für Technologie (KIT), D-76021 Karlsruhe, Germany*

[3]*Institute for Advanced Study, Hong Kong University of Science and Technology, Clear Water Bay, Kowloon, Hong Kong, China*

(Received 23 December 2013; revised manuscript received 10 April 2014; published 6 May 2014)

In this paper, we report a first-principles study of the lattice dynamics of small graphene nanoribbon with zigzag edges. Our investigation is based on spin polarized density functional calculations (DFT). Nesting properties in the electronic band structure are very different for nanoribbons with unpolarized, ferromagnetic, and antiferromagnetic configurations. As a result, the phonon spectrum and nesting related softening in phonon frequencies differ in these cases. The unpolarized and ferromagnetic structures show nesting related phonon softening and considerable electron phonon linewidth, while for the antiferromagnetic structure, a band gap at the Fermi energy eliminates these effects. Saturating the nanoribbon edge with hydrogen has negligible effect on the phonon spectra for the magnetic structures while for the unpolarized configuration all structures without hydrogen are unstable due to soft phonon modes. The electron-phonon coupling coefficients have also been calculated and implications for Peierls transition and superconductivity are discussed.

DOI: 10.1103/PhysRevB.89.205404 PACS number(s): 71.15.Mb, 71.38.−k, 63.22.Rc, 74.10.+v

I. INTRODUCTION

Graphene nanoribbons (GNRs), which are finite strips of two-dimensional (2D) graphene, are attracting a lot of interest. This is partly due to novel properties which have recently been observed in 2D graphene [1–3]. The most remarkable characteristics among these are the existence of massless Dirac electrons at the Fermi level, which show a conelike dispersion at the Dirac point where the conduction band and the valance band touch each other. Going from the 2D graphene to the quasi-one-dimensional nanoribbon allows us to investigate how these unusual effects are influenced by reducing the dimensionality in systems which are periodic only in one dimension while finite in the other one. The reduction in dimensionality gives rise to new phenomena such as magnetic edge states as well as Peierls instabilities [4]. While the electronic structure of nanoribbons has already been investigated and well understood, a detailed study of phonons, electron-phonon coupling effects, and the interplay with magnetic interactions is highly desirable. We focused here on nanoribbons with zigzag edges (ZGNRs), which are the most interesting ones, since tight-binding calculations predict a pair of almost flat bands that exist near the Fermi level within the region $1/3 \leqslant |k| \leqslant 0.5$ (in units of $2\pi/a$, where a is the lattice constant of the graphene nanoribbon along its axis) [5–13]. Flat bands at the Fermi level give rise to strong susceptibilities and may induce instabilities, resulting in lattice distortions, and/or magnetic polarization. Nanoribbons are known to show magnetic effects, manifesting as the spontaneous creation of magnetic edge states [5–13]. The electron spins align ferromagnetically along one zigzag edge, and align in the opposite direction along the other zigzag edge, forming an antiferromagnetic (AF) order (see Fig. 1). Or in other words, the system undergoes a spontaneous spin polarization, which causes electrons at one zigzag edge to be all spin up, and at the other zigzag edge spin down. However, a detailed study has not been carried out for the influence of lattice instabilities and the possible coexistence of both spin magnetic polarization and lattice distortion. With the existence of a Fermi surface, there could be electron-phonon related effects like Peierls distortion and superconductivity, which also could lower the energy. To identify the ground state of a ZGNR, a systematic study which includes magnetic and phononic degrees of freedom is needed.

In this paper, we report first-principles calculation of the lattice dynamics for $N = 2, 4, 6, 8, 10$ ZGNRs, including the spin degree of freedom, to explore the influence of magnetic effects on the phonon spectrum and possible instabilities. The paper is organized as follows. Section II gives the description of the method we use. The next three sections are devoted to studies of hydrogen saturated nanoribbons. Section III describes the electronic band-structure results. For each of the ribbons we have considered the following three situations: (1) the spin unpolarized (SU) case where all electron states are degenerate with respect to the spin; (2) the spin ferromagnetic (FM) case where all spins are aligned in the same direction; (3) the spin antiferromagnetic (AF) case where all electron spins along one ribbon edge are aligned ferromagnetically while across the ribbon the alignment is of opposite direction. The total energy and spin magnetic moment are presented. Nesting vectors between Fermi points in the band structure of spin unpolarized (SU) cases and spin ferromagnetic (FM) cases are identified. In Sec. IV, we show the calculated phonon spectrum, for all these SU, FM, and AF configurations. Electron-phonon interaction induced phonon softening and phonon linewidth at nesting vectors are presented for SU and FM cases. In the AF case, results show that because of the absence of a Fermi surface, the phonon branches are stabilized and phonon linewidth vanishes. In Sec. V, we discuss the electron-phonon coupling in these ZGNR systems. In Sec. VI, we consider the ZGNRs without hydrogen saturation. We show the phonon spectra of nonsaturated ZGNRs to be similar to those with hydrogen saturated except for SU cases, in which the nonsaturated systems are unstable and strong distortions occur. A summary and discussion is presented in Sec. VII.

*Corresponding author: phzting@ust.hk

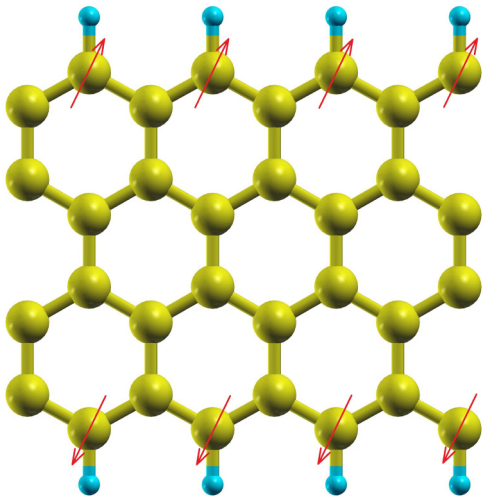

FIG. 1. (Color online) A sketch for $N = 4$ hydrogen saturated nanoribbon, with spin antiferromagnetic aligned along the two zigzag edges. The yellow balls are carbon atoms and blue balls are hydrogen atoms. In the plot hydrogen atoms saturate the edge dangling bonds of the nanoribbon.

II. THEORETICAL METHOD

We employ density functional theory (DFT) to calculate the electronic band structure of the nanoribbons and density functional perturbation theory (DFPT) [13] to study the lattice dynamics and electron-phonon interaction. The DFPT has the advantage that arbitrary points in the Brillouin zone (BZ) can be calculated without the need of using large supercells [14]. This is important for searching for possible instabilities due to structural, magnetic, or electron-phonon coupling effects, which can occur at wave vectors that are incommensurable with the lattice. We use a "mixed-basis" pseudopotential code [15,16], which has already been successfully used for the investigation of nanotubes [17,18] and many other materials. The valance electrons are described by plane waves with a cutoff set to 24 Ryd supplemented by localized $2s$- and $2p$-like local functions. For integrations over the BZ a Gaussian broadening scheme is employed.

The nanoribbons are arranged on a cubic array with 10 $\mathring{A}$ between nearest atoms for different ribbons in the direction perpendicular to the ribbon axis. Such a large distance between the ribbons minimizes inter-ribbon interactions, so that our results are relevant for describing isolated ribbons. Brillouin-zone sampling is done with 256 k points along the ribbon axis and integration is done with a Gaussian width of 0.025 eV. For $N = 2$ nanoribbon we use even up to 2048 k points with Gaussian width of 0.003 125 eV to accurately calculate the energy difference between SU, FM, and AF cases, since for $N = 2$ nanoribbon such values are small and a large k basis is necessary for reducing the numerical errors. For the calculation of phonon dispersion we determine the frequencies on a regular q mesh of nine points along the axis. Interpolation based on these points is supplemented with q points which are dictated by the nesting vectors in the electronic band structure. The nesting vectors are shown in Figs. 3 and in the following. The charge susceptibility is enhanced at these nesting vectors, and the enhanced susceptibility will significantly renormalize the phonon frequencies and induce strong electron-phonon interaction related effects.

III. ELECTRONIC PROPERTIES OF HYDROGEN SATURATED ZGNRS

Before we can examine the phonon dispersion of nanoribbons we have to examine the electronic band structure. We have investigated nanoribbons with a width of $N = 2, 4, 6, 8,$ and 10 (containing $2N$ carbon atoms in the unit cell) where the outermost carbon atoms were saturated with hydrogen to deal with dangling bonds at the ribbon edges. This situation is very different from that of Ref. [19] where all carbon atoms were saturated with hydrogen. Structural optimization led to flat ribbons with optimized carbon-carbon distances. Some authors mentioned that the graphene sheets will undergo spontaneous curling [20], but in our cases, both structural optimization and phonon dispersion calculations confirm that

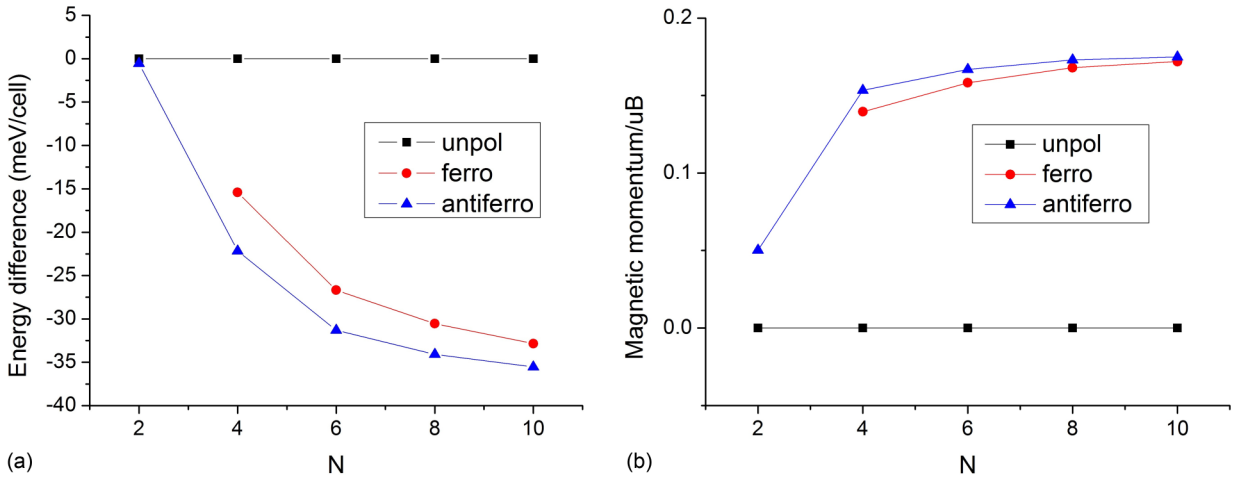

FIG. 2. (Color online) (a) The energy difference of the FM and the AF configurations compared with the SU configuration in saturated ZGNRs, as a function of the width N of the ZGNRs. (b) The maximum magnetic moment of atoms at nanoribbon edge in saturated ZGNRs vs N. Within numerical accuracy no FM configuration could be found for $N = 2$.

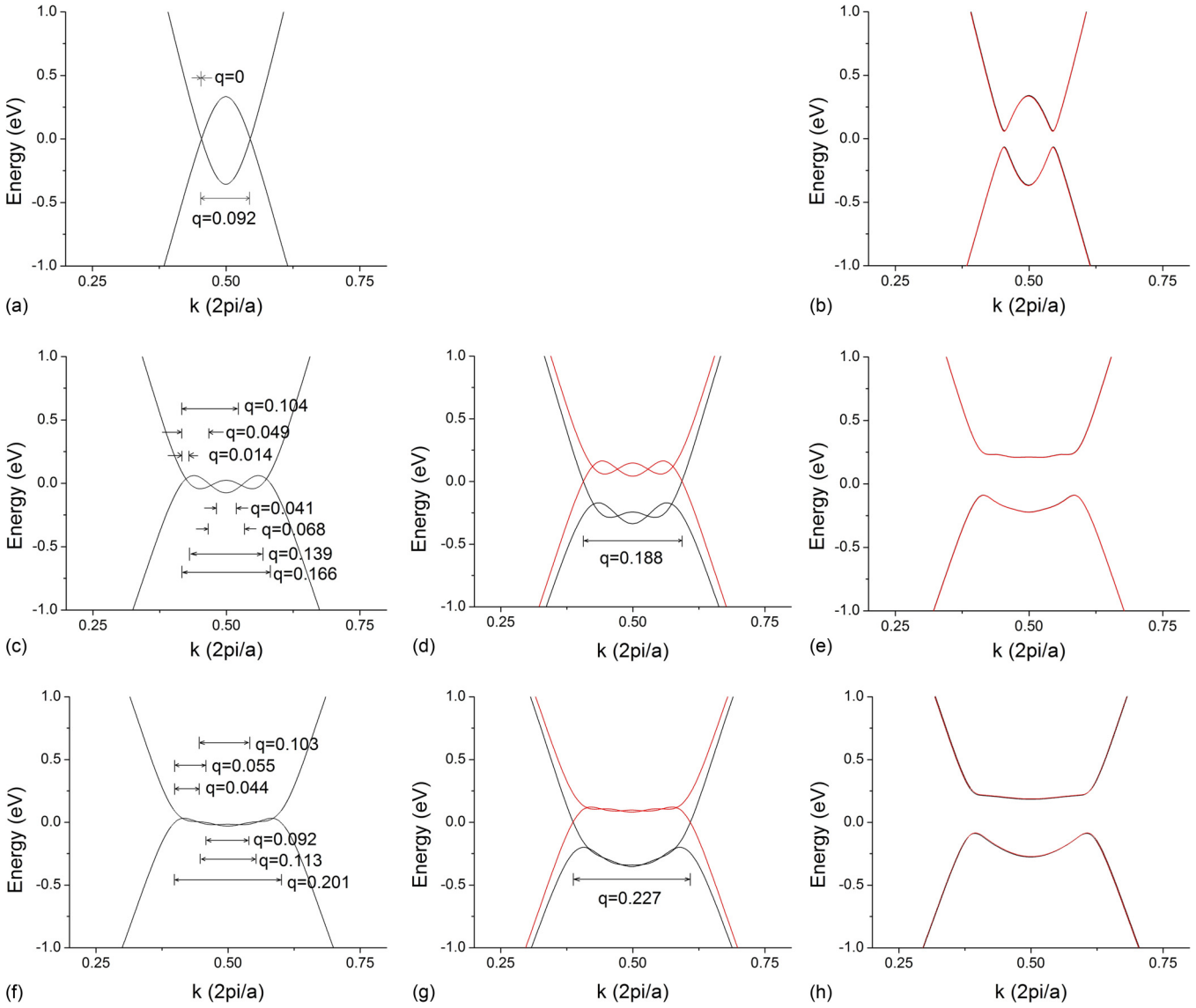

FIG. 3. (Color online) Band structure of $N = 2$, 4, 6 saturated ZGNRs. Panels (a) and (b) belong to $N = 2$ ZGNR, with SU and AF spin configurations, respectively, while panels (c)–(e) belong to $N = 4$ ZGNR, and (f)–(h) belong to $N = 6$ ZGNR. Shown are SU, FM, and AF configurations where red and black colors indicate the spin-up and -down electron branches in spin polarized cases, respectively. Possible nesting vectors are listed in the plots. The Fermi energy is set to zero.

the small ZGNRs should be flat. In structural optimization a flat structure is found to be energetically more favorable than a bending one, and in phonon dispersion there are no soft modes associated to bending of the nanoribbons (see below). In all cases the antiferromagnetic structure showed the lowest energy, while the nonmagnetic structures were energetically most unfavorable. The energy lowering due to spin polarization is shown in Fig. 2(a), with values which vary from ∼0.65 meV/cell for $N = 2$ to ∼36 meV/cell for $N = 10$. With increasing N, the difference between AF and FM configurations decreases. In Fig. 2(b), the magnetic moment for the edge atoms are shown for AF and FM cases as a function of ribbon width, and the saturation moment on the edge atoms is $\sim 0.18 \mu B$.

In Figs. 3(a)–3(h) we have plotted the band structure close to E_f for $N = 2$, 4, and 6 nanoribbons where we have differentiated between the SU, FM, and AF configurations. While SU and FM cases show metallic behavior, the AF structures are gapped. For $N = 2$ we only find a SU and AF state.

TABLE I. The electron-phonon coupling constant λ as defined in Eq. (3) in the text. The antiferromagnetic configurations have gaps and therefore no electron-phonon coupling is obtained. For spin unpolarized cases without hydrogen saturating the edge dangling bonds, the structures are not stable, thus no electron-phonon coupling can be calculated.

	Spin states	λ
$N = 2$, hydrogen saturated nanoribbon	unpolarized	0.14
$N = 4$, hydrogen saturated nanoribbon	unpolarized	0.14
	ferromagnetic	0.077
$N = 6$, hydrogen saturated nanoribbon	unpolarized	0.011
	ferromagnetic	0.039

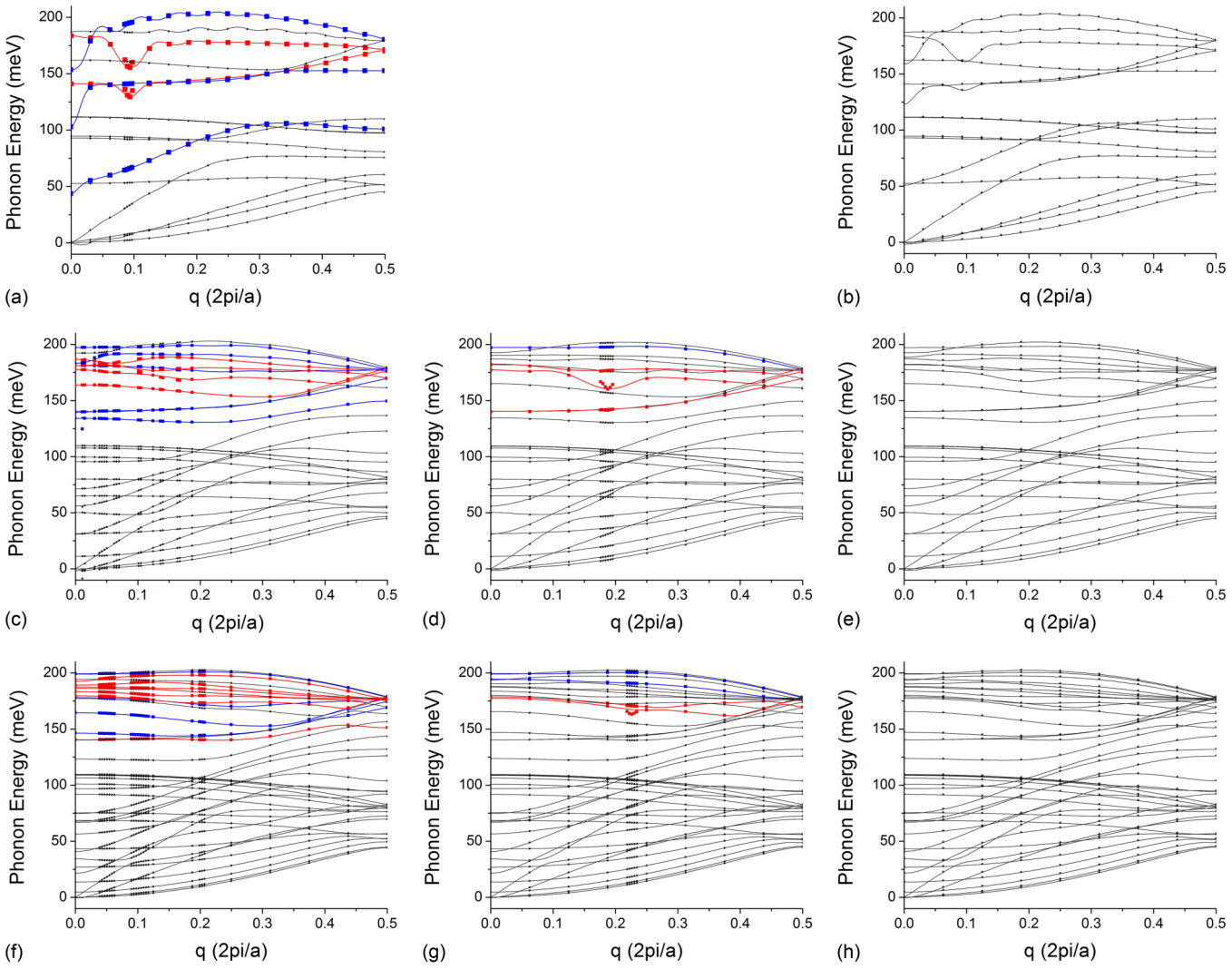

FIG. 4. (Color online) Phonon spectra and el-ph coupling of $N = 2$, 4, 6 saturated ZGNRs, with spin unpolarized, spin ferromagnetic (except $N = 2$ case), and spin antiferromagnetic configurations. The phonon branches with el-ph coupling are highlighted in figures with blue (el-ph coupling at $q = 0$) and red (el-ph coupling at $q = 2k_f$ or other nesting vectors) colors. The dots denote calculated points, and lines are interpolated phonon frequencies. For $N = 2$ plots, the wiggly lines are due to the interpolation of the pronounced anomalies and are unphysical.

It has already been shown previously in a tight-binding study that for SU the edge states play a very important role for nanoribbons [5]. They are located in the region $1/3 \leqslant |k| \leqslant 1/2$ (BZ boundary), and are crossing each other $N/2$ times. This feature can clearly be seen in our results. We have just $N/2$ Fermi points in our calculation for small ribbons while with increasing N due to the negative curvature of the bands the band crossings happen at values away from the Fermi energy ε_f. For larger N we thus have only three Fermi points. Nesting vectors based on these Fermi points are also indicated in Figs. 3(a)–3(h).

For the FM case the situation is very similar to the SU situation but the spin up and spin down bands are no longer degenerate. The edge states with different spins are shifted against each other leading to only one Fermi point per spin.

In contrast the AF structures are very different. Here the two edge states open a gap at ε_f ($\sim$0.1 eV for $N = 2$, and $\sim$0.3 eV for $N > 2$). No Fermi points exist and hence no Fermi surface related instabilities can occur.

IV. PHONON SPECTRUM OF HYDROGEN SATURATED ZGNRS

Phonon dispersions calculated by DFPT for all the nanoribbons discussed so far are presented in Fig. 4. For $N = 2$ and $N = 4$ we see clear indications of phonon softening at nesting vectors for SU and FM situations. Optical phonons soften for $N = 2$ at the Γ point, as well as at the nesting vector $q = 0.0918$. These modes are also those with strong electron-phonon couplings which will be used in the next section to estimate the average electron-phonon coupling which is relevant for superconductivity and Peierls distortion.

The phonon anomalies for $N = 4$ are already much smaller and also the electron phonon coupling approaches very small values. For the SU case we find nine nesting vectors, most of which are too close to the Γ point to be treated reliably without exceptional effort. The larger nesting vectors seem to show no significant phonon softening. For the FM case due to the spin splitting of the bands only one nesting vector survives at $q =$

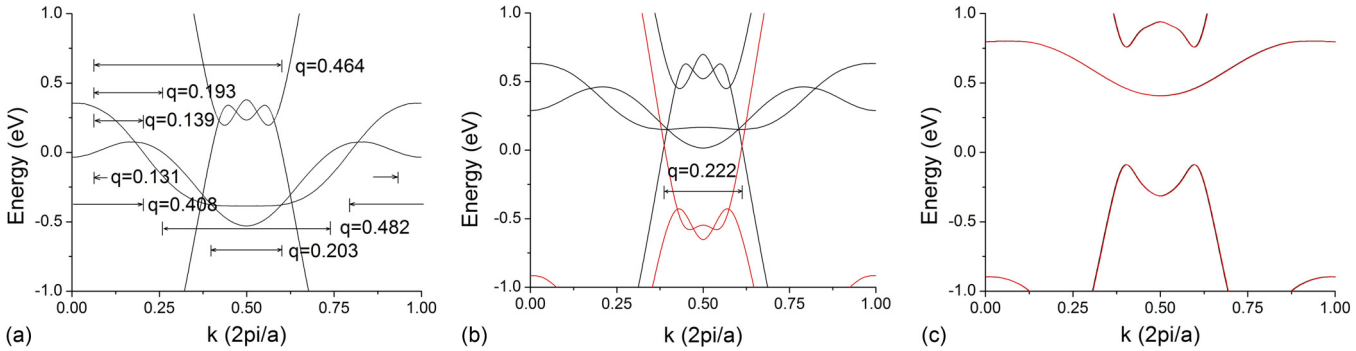

FIG. 5. (Color online) Band structure of (a) SU, (b) FM, and (c) AF spin configurations for $N = 4$ nonsaturated ZGNR.

0.1875. Phonon softening is seen there as expected. For wider ribbons with $N = 6$ we have for the SU situation very weak electron-phonon coupling partially concentrated close to the Γ point with hardly visible phonon softening effects. The FM case shows slightly more pronounced effects. With $N > 6$, phonon anomalies and electron phonon coupling decrease rapidly, thus the phonon dispersions are not presented since they do not show any special effects.

So far we have not discussed the AF structures. For $N = 4$ and 6 we do not see any phonon softening due to the presence of a gap at the Fermi energy.

For $N = 2$ despite the gap opening we still see phonon softening at the Γ point as well as at $q = 0.0918$, but with smaller frequency reduction than in the SU case. This results from the fact that the phonon-frequency renormalization is related to the real part of the phonon self-energy, which depends on scattering of electrons from a finite energy window around the Fermi level and thus can occur even in the absence of a Fermi surface [21].

V. ELECTRON-PHONON INTERACTION RELATED PROPERTIES IN ZGNRS

So far we have discussed only the phonon dispersion including electron-phonon interactions. To investigate the possibility of phonon induced superconductivity, we have calculated the microscopic electron-phonon coupling parameters which are central to the Eliashberg theory of strong-coupling superconductors. The coupling constant for a phonon mode q,ν is given by

$$\lambda_{q,\nu} = \frac{2}{\hbar N(\varepsilon_f)\omega_{q,\nu}} \sum_{k,i,i'} \left| g^{q\nu}_{k+q,i';k,i} \right|^2 \delta(\varepsilon_{k,i})\delta(\varepsilon_{k+q,i'}), \quad (1)$$

where $N(\varepsilon_f)$ is the density of states at the Fermi energy and all energies are measured with respect to ε_f, and i denotes the band index. The electron phonon matrix element is given by

$$g^{q\nu}_{k+qi';ki} \propto \langle \phi_{k+qi'} | \delta V^{q\nu}_{\text{eff}} | \phi_{ki} \rangle, \quad (2)$$

where $\delta V^{q\nu}_{\text{eff}}$ is the crystal potential change due to the phonon q, ν and ϕ_{ki} is the electron wave function. The total coupling constant is given by

$$\lambda = \frac{1}{N_q} \sum_{q,\nu} \lambda_{q,\nu}, \quad (3)$$

where N_q is the number of q points.

As the Fermi surface of these ribbons consists only of a few k points, contribution to the total electron-phonon coupling constant λ is restricted to the nesting vectors. Table I shows rough estimates for the SU $N = 2, 4, 6$ cases and FM $N = 4$ and $N = 6$ cases saturated with hydrogen. For $N > 6$ no significant λ can be obtained.

We also investigated the influence of doping the AF case for $N = 2$. This was guided by the electronic band structure which showed only a small gap indicating that weak electron doping should allow for shifting the Fermi energy to the bottom of the conduction band. The high density of states supported the expectation of large electron-phonon coupling. Assuming a rigid-band picture we obtained values similar to the SU configuration for $N = 2$, but these values were dependent on the numerical treatment. Going beyond the rigid-band picture we found that already for small doping the band structure was modified such that the gap was closed and the AF state no longer survived. This is not surprising in view of the small energy gain which favors the undoped AF state for $N = 2$ over the corresponding SU state. We thus conclude that doping the $N = 2$ AF state does not give rise to large electron-phonon interaction.

To assess the importance of magnetic effects as compared to the Peierls instability, we have estimated the Peierls transition temperature for the SU structure $N = 2$. By fitting the frequency dependence of the optical soft phonons at $q = 0$ and $q = 0.0918$ with respect to different level broadening, or Gaussian smearing corresponding to different temperatures, we can calculate the Peierls transition temperature with the equation (see also Ref. [16] for the smearing and temperature correspondence)

$$(\hbar\omega_{q,\nu})^2 = A_{q,\nu} \ln\left(\frac{T}{T_p}\right), \quad (4)$$

where $\hbar\omega_{q,\nu}$ is the energy of the phonon q, ν which gets soft in cooling process, and T_p is the Peierls transition temperature of the phonon mode. We obtained a maximum transition temperature of $T_p \sim 18$ K and a prefactor $A \sim 868$ (meV)^2 for the phonon mode at the Γ point. This mode is about 44 meV when the level broadening is 0.025 eV. Since this value of T_p is reasonably large, the Peierls state might therefore compete with the AF state.

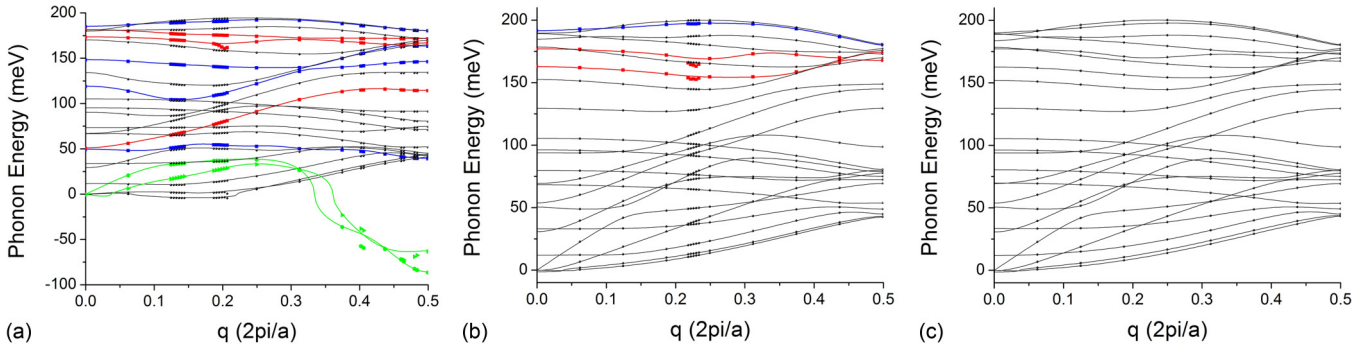

FIG. 6. (Color online) Phonon spectrum of $N = 4$ nonsaturated ZGNRs. Panels (a)–(c) are for SU, FM, and AF configurations, while for $N = 6$ ZGNR, no new features are observed and the results are not shown. The color definitions are the same as in Fig. 4. The phonon branches in green color mean the system is unstable for those oscillations.

VI. ELECTRONIC AND PHONONIC PROPERTIES OF NONSATURATED ZGNRS

Having considered ribbons saturated with hydrogen, we summarize for completeness the main differences for cases without hydrogen saturation. The dangling bonds change the electronic structure dramatically. For $N = 2$, we cannot find stable configurations. For $N = 4$ and 6, we find significantly larger spin-polarization influences, larger energy gains, and larger magnetic moments at the edge atom of $\sim 0.85 \mu B$. The band structure shows two bands close to the Fermi energy which are related to the dangling bonds and strongly influence the electronic properties. For the SU case these bands are located at E_f and lead to new nesting vectors and strong renormalization effects. In the FM case these bands are spin split while for the AF structures they interact and open a gap, and hence no new nesting vectors are generated. Results for $N = 4$ are shown in Fig. 5. The phonon spectrum for the SU case, Fig. 6(a), shows large regions of instability close to the zone boundary. In this situation we considered a reconstructed dimerization cell which led to a stabilization of the structure but the energy gain was found to be smaller than that due to spin polarization. For the FM and AF cases, stable phonon spectra have been observed. This is due to the fact that the dangling-bond bands are located away from the Fermi energy and thus induce only a minor effect. Here the unsaturated as well as saturated ribbons behave very similarly. A closer look at Fig. 6 where all the phonon dispersions are presented reveals some phonon softening for FM with $N = 4$. Results for $N = 6$ are very similar with even weaker softening effects for the FM case and are thus not shown.

VII. SUMMARY AND DISCUSSION

In summary, we perform first-principles calculation on electronic and phonon related properties of ZGNRs. Band structures, phonon spectra, and electron-phonon couplings for different ZGNRs are calculated. By taking the spin degree of freedom into account, a systematic comparison of different spin configurations, namely the spin unpolarized, the spin ferromagnetic, and the spin antiferromagnetic configurations, for the two edge states in ZGNR is performed. We find that the electronic structure near the Fermi energy is greatly influenced by spin configurations, and therefore lattice dynamics is tightly connected with the spin states. Our calculations lead to an understanding of the electronic and phononic properties of small ZGNRs. In spin unpolarized and ferromagnetic cases, electron-phonon interaction induced phonon softenings are observed at corresponding nesting q vectors, and the softening decreases with increasing width of the nanoribbon. In spin antiferromagnetic cases, because of the gap opening in the band structure, all Fermi-surface related electron-phonon interaction effects (e.g., linewidth) vanish. For $N = 2$ saturated ZGNR, doping can possibly induce electron-phonon interaction in the spin AF setting but this is sensitive to the actual doping level and details of the numerical treatment. This is explained by the small energy gain in $N = 2$ ZGNR from spin antiferromagnetic ordering due to a very small moment at the atoms. Since for $N = 2$ the electron-phonon coupling in the SU case is strong this might be a possible case where Peierls distortion or even superconductivity can compete with the antiferromagnetic ordering and thus could influence the ground state of the $N = 2$ nanoribbon. For all other cases considered here the energy gain due to electron-phonon coupling is small compared with the gain due to the antiferromagnetic ordering of the edge states.

We note that these results for the nanoribbons are very different from results for small nanotubes. For example, a substantial electron-phonon coupling has been obtained for (3,3) nanotubes with 12 atoms in the unit cell [16]. Since the nanoribbons considered here are exhibit even stronger one-dimensional characteristic than carbon nanotubes (which is known to have strong electron-phonon interaction), one might have expected even stronger effects for the nanoribbons. It is known however from nanotube studies that electron-phonon coupling increases with curvature [22]. In addition our results are also in agreement with a tight-binding study where the smaller effects in the nanoribbons are related to the higher symmetry which leads to the disappearance of many electron-phonon matrix elements [22]. The absence of curvature and the higher symmetry in ribbons make the lattice instability weak compared with Stoner instability.

ACKNOWLEDGMENTS

This work is supported by Hong Kong Research Grant Council Grant No. AoE/P-02/12, HKUST9/CRF/08, and SRFI11/SC02. The authors are grateful to Professor S. G.

Louie for valuable discussions. T.Z. thanks KIT for the hospitality during his stay in Karlsruhe. The authors are grateful to the National Supercomputing Center in Shen Zhen for computational resources.

[1] D. S. L. Abergel, V. Apalkov, J. Berashevich, K. Ziegler, and T. Chakraborty. Adv. Phys. **59**, 261 (2010).
[2] A. K. Geim, Science **324**, 1530 (2009).
[3] M. J. Allen, V. C. Tung, and R. B. Kaner, Chem. Rev. **110**, 132 (2010).
[4] R. Peierls, *Quantum Theory of Solid* (Clarendon, London, 2001).
[5] M. Fujita, K. Wakabayashi, K. Nakada, and K. J. Kusakabe, J. Phys. Soc. Jpn. **65**, 1920 (1996).
[6] K. Nakada, M. Fujita, G. Dresselhaus, and M. S. Dresselhaus, Phys. Rev. B **54**, 17954 (1996).
[7] M. Fujita, M. Igami, and K. Nakada, J. Phys. Soc. Jpn. **66**, 1864 (1997).
[8] Y. Miyamoto, K. Nakada, and M. Fujita, Phys. Rev. B **59**, 9858 (1999).
[9] Y. Miyamoto, K. Nakada, and M. Fujita, Phys. Rev. B **60**, 16211 (1999).
[10] K. Kusakabe and M. Maruyama, Phys. Rev. B **67**, 092406 (2003).
[11] A. Yamashiro, Y. Shimoi, K. Harigaya, and K. Wakabayashi, Phys. Rev. B **68**, 193410 (2003).
[12] H. Lee, Y.-W. Son, N. Park, S. Han, and J. Yu, Phys. Rev. B **72**, 174431 (2005).
[13] L. Pisani, J. A. Chan, B. Montanari, and N. M. Harrison, Phys. Rev. B **75**, 064418 (2007).
[14] S. Baroni, P. Giannozzi, and A. Testa, Phys. Rev. Lett. **58**, 1861 (1987).
[15] B. Meyer, C. Elsaesser and M. Faehnle, FORTRAN90 Program for Mixed-Basis Pseudopotential Calculations for Crystals, Max-Planck-Institut for Metallforschung, Stuttgart (unpublished).
[16] R. Heid and K. P. Bohnen, Phys. Rev. B **60**, R3709 (1999).
[17] K.-P. Bohnen, R. Heid, H. J. Liu, and C. T. Chan, Phys. Rev. Lett. **93**, 245501 (2004).
[18] K. P. Bohnen, R. Heid, and C. T. Chan, Phys. Rev. B **77**, 235407 (2008).
[19] H. Sahin, C. Ataca, and S. Ciraci, Phys. Rev. B **81**, 205417 (2010).
[20] V. B. Shenoy, C. D. Reddy, and Y. W. Zhang, ACS Nano. **4**, 4840 (2010).
[21] R. Barnett, E. Demler, and E. Kaxiras, Phys. Rev. B **71**, 035429 (2005).
[22] L. X. Benedict, V. H. Crespi, S. G. Louie, and M. L. Cohen, Phys. Rev. B **52**, 14935 (1995).